J. Fluid Mech. (2000), *vol.* 402, *pp.* 211–223. Printed in the United Kingdom

Scattering of an eddy advected by a current towards a topographic obstacle

By MELVIN E. STERN

Oceanography Department(4320), Florida State University, Tallahassee, FL 32306-4320, USA
e-mail: stern@ocean.fsu.edu

(Received 13 May 1999 and in revised form 5 August 1999)

Contour dynamics is used to compute the two-dimensional (f-plane) motion of an initially circularly symmetric barotropic eddy with piecewise-uniform vorticity as it is advected around a circular obstacle by a uniform upstream current. For grazing incidence of this 'shielded' eddy (compensating positive and negative vorticity) the main effect of the vortex images (inside the obstacle) is to change the speed of those particles in the outer portion of the eddy that are closest to the obstacle; a lesser velocity is induced on the oppositely signed vortices near the eddy centre. The result is a systematic separation of the centroids of the $\pm$ vortices in the eddy, and the eddy emerges far downstream with an invariant dipole moment ($m = 1$ azimuthal mode). This causes the eddy to move with a constant velocity V normal to the uniform basic flow. The ratio of the numerically computed V to the accompanying far-field dipole moment agrees with a previous analytical theory for a completely isolated eddy subjected to a small-amplitude $m = 1$ initial disturbance. The scattering effect might be realizable in a rotating homogeneous fluid by translating a cylinder relative to an otherwise stationary eddy. Application to a density-stratified model is suggested.

1. Introduction

If $z_I = x+\mathrm{i}y$ denotes the complex position vector of the Ith point vortex of strength $2\pi G_I$ in an inviscid and unbounded two-dimensional flow, then it follows from the equation of motion for $\mathrm{d}z_I/\mathrm{d}t$ that the 'dipole moment', defined to be proportional to

$$\sum_1^N G_I z_I(t),$$

is time independent (Saffman 1992). Also well known is the generalization for distributed vorticity $\omega(x, y, t)$ in a 'compact eddy' where the vector invariant is

$$\iint \mathrm{d}x\,\mathrm{d}y(\omega x, \omega y),$$

and the integration extends over the entire two-dimensional f-plane. The simplest case for further consideration consists of a piecewise-uniform-vorticity eddy, consisting of an inner domain with uniform vorticity ω_3 and an area A_3; this is bounded by an interfacial contour $(C_3(t))$ whose centroid is located at $(x_3(t), y_3(t))$. Outside C_3 there is an annular domain of vorticity ω_2 in an area $A_2 - A_3$ which is bounded by a closed contour $C_2(t)$ whose centroid is at $(x_2(t), y_2(t))$; outside C_2 the vorticity vanishes. The 'shielding' requirement is $\omega_3 A_3 + \omega_2(A_2 - A_3) = 0$, and the invariant dipole moment therefore has the x-component

$$\omega_3 A_3 x_3 + \omega_2[x_2 A_2 - x_3 A_3] = \omega_2 A_2(x_2 - x_3).$$

Thus we see that the distance

$$\boldsymbol{D} = (D_x, D_y) = (x_2 - x_3, y_2 - y_3) \tag{1.1}$$

between the centroids is time invariant, in the absence of external forces, such as may be provided by rigid boundaries or by the latitudinal variation of the Coriolis force.

When such forces are absent, then a ‘small’ initial D_x will cause this ‘almost’ circularly symmetric eddy to propagate in the $+y$-direction with speed

$$V = \tfrac{1}{2} D_x \omega_2, \tag{1.2}$$

and for a time such that the eddy is able to traverse many diameters (Stern & Radko 1998, equation (2.2)). This reference also examines the collision of such a self-propagating eddy with the interface bounding a semi-infinite laminar shear flow with piecewise-uniform vorticity. Under certain conditions the dipole moment of the eddy enables it to completely penetrate the barrier provided by the vorticity discontinuity at the interface of the shear flow. This suggests the importance of the small dipole moment for mixing an eddy with a current having different properties.

The purpose of this paper is to show how the foregoing (1.1) f-plane invariant can be generated, i.e. how an initially circularly symmetric eddy can acquire a dipole moment as a result of the pressure exerted on a topographic obstacle, such as a circular cylinder of radius R centred at $x = 0 = y$. Far upstream ($x = -\infty$) this eddy with its centre at $x = -\infty$, $y = y_3(0)$ is advected towards the obstacle by the uniform velocity U of a basic current. Further downstream the irrotational U-flow around the obstacle distorts the interfaces (C_2, C_3), and ‘activates’ the image vorticies inside the obstacle. The main dynamical effect of the latter occurs when C_2 and its proximate particles are sufficiently close to the obstacle, so that their velocity is significantly modified by the closeness of images. Since the images have less effect on the more distant C_3 contour, we expect the centroids of C_2 and C_3 to separate, thereby producing a finite value of (1.1). The main question to be answered is whether the effect is reversible, or whether it causes a finite D to appear far downstream from the obstacle. In the latter case the eddy will have a constant propagation velocity (1.2) normal to the basic flow. Attention will be mainly confined to the ‘weak scattering’ regime, wherein the magnitude of the upstream ordinate of the eddy centre is such that C_2 ‘grazes’ the obstacle and emerges far downstream as a simply connected round curve (i.e. no ‘topological change’), but with a finite scattering angle relative to U. The ‘strong’ interaction regime, on the other hand is defined by the presence of a topological change such as a bifurcation into two essentially separated eddies, or such as results from a ‘head-on’ collision of C_2 with the obstacle. The subsequent evolution of this case is beyond our scope, and at the time when this effect occurs our contour dynamical calculations (§ 4) are terminated.

From an oceanographic point of view, however, both regimes are of interest, as appears in the Richardson & Tychensky (1998) observations of ‘Meddies’ propagating southwestward from their origin on the Iberian continental slope. Some of these come into close contact with mid-Atlantic topography, and either change their propagation direction (weak scattering), or become disrupted into smaller scale structures (strong interaction). If the latter speculation of Richardson & Tychensky (1998) is correct, it has important implications for mixing the high-salinity Meddies in the much larger water mass in which they are embedded. The question then arises as to the relevance of our pure, barotropic considerations to the ocean, which is vertically stratified in density. The simplest baroclinic case is a two-layer quasi-geostrophic model, and we show (§ 5) how the foregoing barotropic centroid invariant generalizes to that case. It will be suggested that a sea mount can cause an initially symmetric eddy to acquire such an invariant. See Beismann, Käse & Lutejeharms (1999) for the effect of a uniform north–south ridge on a westward-propagating β-plane eddy.

The simpler barotropic problem considered herein is also of interest because it may be realizable in a laboratory experiment with a rotating fluid of uniform density. Compact eddies have been produced by S. Vorapayev (1999, personal communication) and Carnevale, Kloosterziel & van Heijst (1991), and the latter have studied numerically, as well as experimentally, the evolution of an eddy on the β-plane. The question addressed here is what happens when a rigid cylinder on the f-plane is moved towards an initially circularly symmetric eddy with no net circulation.

The simplest model (§ 2) which elucidates this topographic effect consists of an eddy composed of only three point vortices, with no net circulation, and such that in the absence of rigid boundaries it is in a stable rotary equilibrium state (Rott 1989). When a circular obstacle and a basic current are added, a relatively simple point vortex calculation gives the positions of the three vortices as they are advected around the obstacle, and as they emerge far downstream.

The problem is generalized in § 3, where we consider an eddy with piecewise-uniform vorticity. The simplest version of this occurs when the aforementioned inner C_3 contour collapses to a point $(x_3, y_3(t))$ surrounded by the distributed vorticity inside C_2. In order to compute the evolution of C_2, and $x_3(t), y_3(t)$, it is necessary to obtain the velocities induced by the vortex images. The Green's function for these images is, however, not Galilean invariant, and therefore does not allow a reduction of the two-dimensional problem to a one-dimensional calculation (as in conventional contour dynamics). Consequently the numerics in § 3 require a two-dimensional integration over the entire area bounded by C_2 in order to obtain the velocity induced by their images. The results of these calculations are discussed in § 4, and summarized in the conclusion. In § 5 the aforementioned (barotropic) centroid invariance theorem is generalized to a baroclinic model.

2. A simple explanation of the weak scattering effect

Consider a shielded eddy consisting of a central cyclonic vortex, with non-dimensional strength $G_3 = +\frac{2}{3}$ (multiplied by 2π), initially separated by unit distance from two co-linear anticyclones whose strength is $G_1 = G_2 = -\frac{1}{3}$ (multiplied by 2π). The respective positions at $t = 0$ of this special eddy are $z_1(0) = x_1 + \mathrm{i}y_1, z_2(0) = z_1(0) + 2\mathrm{i}$, $z_3(0) = (z_1 + z_2)/2$. When $U = 0$ there is an elementary stable solution (Rott 1989) in which the two negative satellites merely rotate counterclockwise with angular velocity $\frac{3}{2}$ about a fixed z_3.

Now suppose there is a circular obstacle of non-dimensional radius R centred at $x = 0, y = 0$, and at $x = -\infty$ there is a non-dimensional uniform basic current U. This irrotational flow will advect each point vortex towards and around the circle. Each vortex ($I = 1, 2, 3$) is also directly influenced by the remaining two, and indirectly influenced by all three image vortices inside the circular obstacle. The sum of these three influences gives the well known equations of motion:

$$\frac{\mathrm{d}z_I}{\mathrm{d}t} = \sum_{J \neq I} \frac{\mathrm{i}G_j}{z_I^* - z_j^*} - \sum \frac{\mathrm{i}G_j}{z_I^* - (R^2/z_J)} + U[1 - (R^2/(z_J^*)^2)], \tag{2.1}$$

where the asterisk denotes a complex conjugate. Note that vanishing circulation around the circular obstacle is ensured by the compensating strength of the three images. Many different and intricate trajectories can be obtained, depending on the (U, R) parameter and on $y_3(0)$. The example chosen below best illustrates the weak scattering effect which occurs (§ 4) for distributed vortices.

The trajectories (figure 1) of the three vortices for $R = 1$, $U = 0.2$, $x_3(0) = -4$, $y_1(0) = 0.8$ were obtained using a second-order Runge–Kutta integration with a time step = 0.001. After flowing around the obstacle they emerge with a finite 'scattering angle' relative to the direction of the basic flow. This effect is due to the images which become important when the circular obstacle is close to one (z_1 or z_2) of the negative satellites, in which case its azimuthal velocity is retarded by the closeness of its image. The image effect on the central vortex (z_3) is much less because of its much larger separation from the circle, and thus the centroid $[(z_1 + z_2)/2]$ of the negative vortices lags slightly behind z_3 as the entire group flows around the obstacle. Figure 1(c) shows that the x-component of the dipole moment:

$$\sum G_I x_I, \tag{2.2}$$

increases systematically from its upstream value (zero) to an invariant positive downstream ($x \gg R$) value. The y-component of the dipole moment (figure 1c) is, however, much smaller. Also note that no dipole moment forms when $-x_3$ is as large as 4.0.

3. Formulation of the contour dynamical equations for piecewise-uniform vorticity

Let the centre of the circular obstacle with radius R be at the coordinate origin ($x = 0$, $y = 0$), and consider a circularly symmetric shielded (no net vorticity) eddy initially in stable equilibrium at $x = -\infty$. Such is the case for a piecewise-uniform vorticity distribution (Flierl 1988), in which the radius of the inner interface (C_3) is less than half the radius of the outer interface (C_2). For maximum simplicity, in that which follows, the inner domain is taken to be a point vortex located at ($x_3(t)$, $y_3(t)$), with G now denoting its strength (integrated vorticity). This point vortex is surrounded by uniform vorticity $\omega = -G/A$, where A is the area bounded by $C_2(t)$, and $[\overline{x}(t), \overline{y}(t)]$ is its centroid. A uniform current at $x = -\infty$ advects the initially symmetric eddy towards the obstacle.

The total vector velocity $u + \mathrm{i}v$ at any point (x, y) can be expressed as the sum of several components. As in (2.1) one of these:

$$U_a + \mathrm{i}V_a = U(1 - (R^2/(x - \mathrm{i}y)^2)) \tag{3.1}$$

is due to the irrotational flow of the basic current around the obstacle. Another component comes from the point vortex at $z_3 = x_3 + \mathrm{i}y_3$ and from its image at $z_4 = x_4 + \mathrm{i}y_4$:

$$U_3 + \mathrm{i}V_3 = \frac{\mathrm{i}G/2\pi}{(x - x_3) - \mathrm{i}(y - y_3)}, \tag{3.2a}$$

$$U_4 + \mathrm{i}V_4 = \frac{-\mathrm{i}G/2\pi}{(x - x_4) - \mathrm{i}(y - y_4)}, \tag{3.2b}$$

where

$$z_4 = \frac{R^2}{z_3^*} \equiv \frac{R^2}{x_3 - \mathrm{i}y_3}. \tag{3.2c}$$

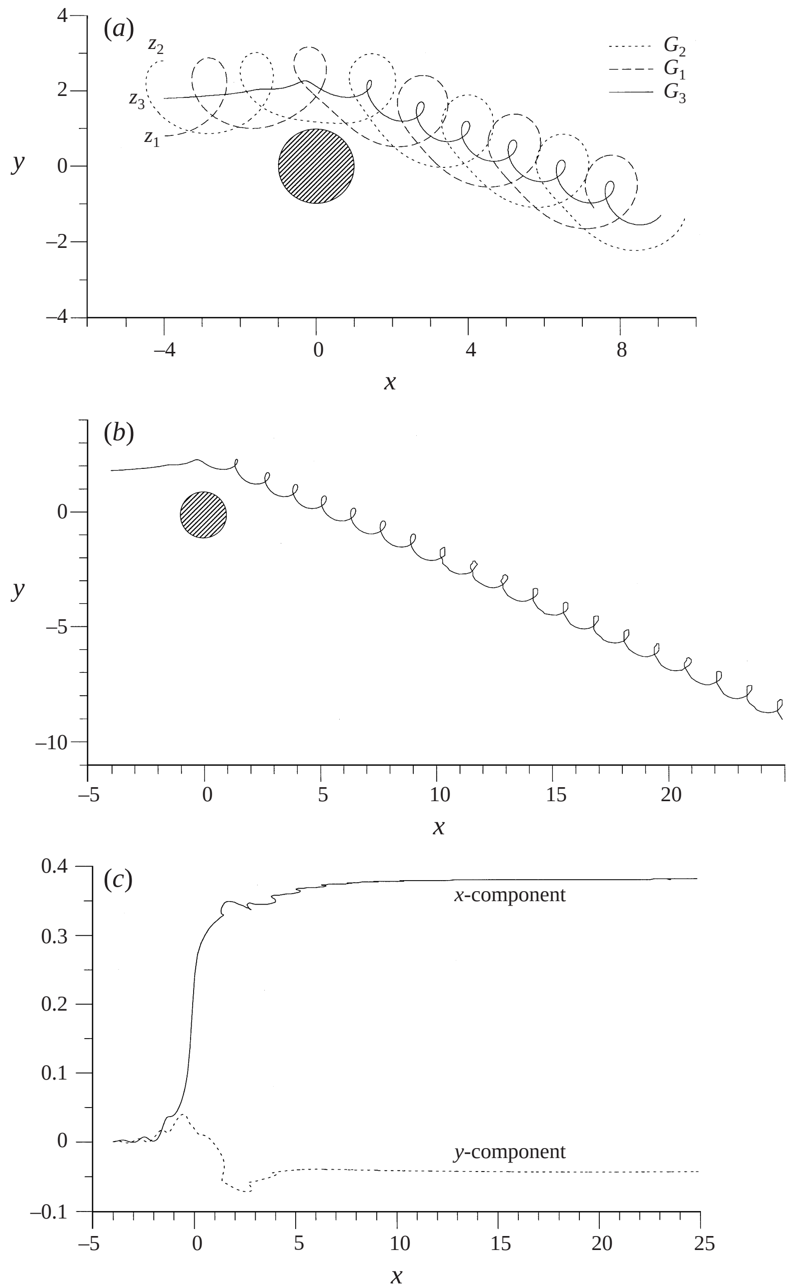

FIGURE 1. (*a*) Three compensating point vortices are advected by a uniform upstream flow towards a circular obstacle, where they are deflected by their images and by the irrotational flow around the obstacle .The central vortex z_3 is positive and its strength (G_3) is twice that of the negative satellites. $U = 0.2$, $R = 1$ (see text). (*b*) The long-time behaviour of the central vortex (compare with propagating three-vortex solution in figure 14 of Rott 1989) shows that a large and persistent 'scattering angle' occurs. (*c*) The downstream evolution of the dipole moment (ordinate); the x-component defined by (2.2) clearly predominates. Note that no dipole moment is generated near the starting position $x = -4 \approx -\infty$.

Conventional contour dynamics enables us to express the direct influence ($U_{ed} + \mathrm{i}V_{ed}$) of all the ω-vortices inside the area bounded by C_2 by a one-dimensional integral:

$$U_{ed} + \mathrm{i}V_{ed} = \frac{\omega}{4\pi} \oint_{C_2} (\mathrm{d}x_J + \mathrm{i}\mathrm{d}y_J) \ln[(x - x_J)^2 + (y - y_J)^2]. \tag{3.3}$$

We evaluated this numerically using the same code as in Stern & Radko (1998), wherein the propagation speed of an isolated eddy with an assumed small dipole moment was computed.

The final and most complicated component ($U_{IM} + \mathrm{i}V_{IM}$) is the velocity produced by the images of the ω-vortices. The double integral over A of the Green's function cannot, as seen below, be reduced to a one-dimensional contour integral. From the streamfunction for a vortex element $\omega\, \mathrm{d}\xi\, \mathrm{d}\eta$ in A we obtain

$$U_{IM} + \mathrm{i}V_{IM} = \frac{\omega}{4\pi} \left(\mathrm{i}\frac{\partial}{\partial x} - \frac{\partial}{\partial y} \right) \iint_A \mathrm{d}\xi\, \mathrm{d}\eta \ln \left| z - \frac{R^2}{\zeta^*} \right|,$$

where $\zeta^* = \xi - \mathrm{i}\eta$. Simplification then yields

$$U_{IM} + \mathrm{i}V_{IM} = \frac{\omega}{2\pi} \iint_A \mathrm{d}\xi\ \mathrm{d}\eta \frac{(x + a)\mathrm{i} - (y + b)}{(x + a)^2 + (y + b)^2}, \tag{3.4}$$

where

$$a = -\frac{R^2 \xi}{\xi^2 + \eta^2}, \quad b = -\frac{R^2 \eta}{\xi^2 + \eta^2}. \tag{3.5}$$

The sum of (3.5), (3.1)–(3.3) evaluated at Lagrangian contour points z_2 on C_2 (with due consideration for the logarithmic singularity) gives $\mathrm{d}z_2/\mathrm{d}t; \mathrm{d}z_3/\mathrm{d}t$ is obtained from the velocity components at $z_3 = x_3 + \mathrm{i}y_3$.

The double spatial integration (3.4) was performed by starting with successive points (ξ_J, y_J) on C_2, where ξ_J is the abscissa and $y_J(\xi_J)$ is the ordinate relative to the centroid $\overline{y}$. If $y_J > 0$ the η-integration proceeds downwards to $\eta = 0$, and if $y_J < 0$ the η-integration is upwards to $\eta = 0$. This procedure allows the area covered at each of the C_2 points to be included in the same simple way. We then sum over ξ_J to obtain the value of (3.4) at any point (x, y) on C_2, and also at $x_3(t)$, $y_3(t)$. To test the algorithm we set $U = 0$, and placed the interface (C_2) of the circularly symmetric eddy outside the obstacle. This should not disturb the equilibrium of the shielded eddy, as was verified by showing that the numerical value (3.4) of the ω-images at $z = z_3$ is equal and opposite to that (3.2*b*) due to the point vortex image.

In the initial state ($t = 0$) of the following calculations ($U > 0$) 80 Lagrangian points were uniformly disturbed around C_2. At $t > 0$ a point was deleted (inserted) if it got too close to (far apart from) a neighbour. Such 'contour surgery' introduces small changes in area (A) in each time step, and, in order to maintain zero net circulation, a (small) compensation in G was made such that $G(t) = -\omega A(t)$ at all time (see Stern & Radko (1998) where a similar procedure was used). A second-order Runge–Kutta scheme was employed with a time step such that the eddy advanced a distance of 0.02 radii in this interval.

4. Results of contour dynamical calculations

At early times (when $-x_3 \gg R$) the compensating vortices ($\pm$) inside C_2 induce negligible net exterior velocity; the dominant effect on the eddy is merely a uniform downstream advection, followed by the straining associated with the irrotational basic

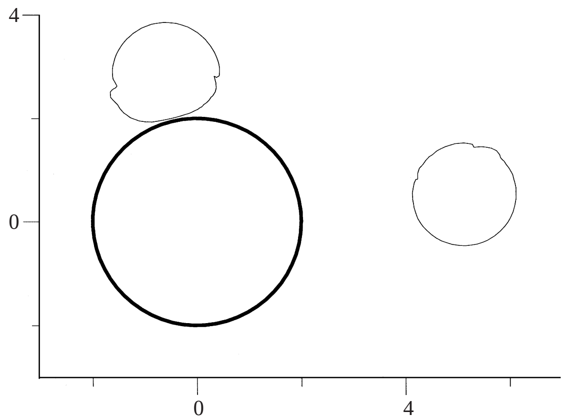

FIGURE 2. A cyclonically rotating eddy with piecewise-uniform vorticity, is advected around a circular obstacle (thick curve of radius $R = 2$) centred at $x = 0$, $y = 0$. At $t = 0$ (not shown) the centroid of the eddy contour (C_2) and the central point vortex ($G = -\pi\omega$) are at $x = -4$, $y = 2$, and the basic current is $U = 0.2$ (see text). The C_2 contours at time $t = 16$ and $t = 50$ are shown here.

flow (U) around the circle of radius R. As in § 2, dynamically significant modifications occur when a segment of $C_2(t)$ (and its neighbouring ω-vortices) comes 'close' to the circular obstacle. The corresponding vortex images then have a dominant effect on those close vortices, and alter the velocity with which those vortices move around the obstacle. Since the total image effect on the more distant point vortex (x_3, y_3) is much less, it will separate from the C_2-centroid by a vector distance $[x_3(t)-\bar{x}(t), y_3(t)-\bar{y}(t)]$. For convenience this is defined as the dipole moment in that which follows.

The equations of motion in § 3 were non-dimensionalized by taking $C_2(0)$ to be a circle of unit radius ($R = 1$) which bounds non-dimensional vorticity $\omega = -2$. Initially the compensating point vortex (x_3, y_3) of strength $G = -\pi\omega$ coincided with the centroid of $C_2[x_3(0) = \bar{x}(0)]$. Although $\omega < 0$ corresponds to a cyclonically rotating eddy, there is no loss of generality since the solution for an anticyclone may be obtained from the class of cyclonic solutions by merely changing the sign of $[y_3(0), \bar{y}(0), \omega, G]$. Note that a cyclonic eddy incident on the left-hand side of the obstacle (looking downstream) behaves differently from a right-hand arrival, because in each case the 'close' images induce azimuthal velocities on C_2 which are in a different sense relative to direction of the basic current (i.e. (3.1)). Each right-hand anticyclonic arrival is, as mentioned above, isomorphic with a left-hand cyclonic arrival, as may be seen by viewing an evolution from below the (x, y)-plane, as well as from above.

In all the following calculations we took $x_3(0) = \bar{x}(0) = -4$, since smaller values merely produced a uniformly translating C_2. Figure 2 shows the position of $C_2(16)$ and $C_2(50)$ for $y_3(0) = \bar{y}(0) = 2$, $U = 0.2$, $R = 2$. Note the well-known shear straining and wave steepening effect ($t = 16$) associated with the wavelet on C_2. If contour surgery were not used in this calculation the further development of this effect would lead to long, thin, and dynamically negligible filaments (tips) winding continuously around the eddy centre. Since this would either compromise the numerical resolution or require excessive computational time, a 'tip' point in a filament was removed (and C_2 reconnected) if the distance between its two neighbours was too small (cf. Stern & Radko 1998). This procedure can lead to a small (but systematic) increase in the area bounded by C_2, and in the total strength of its ω-vortices; and (as mentioned above)

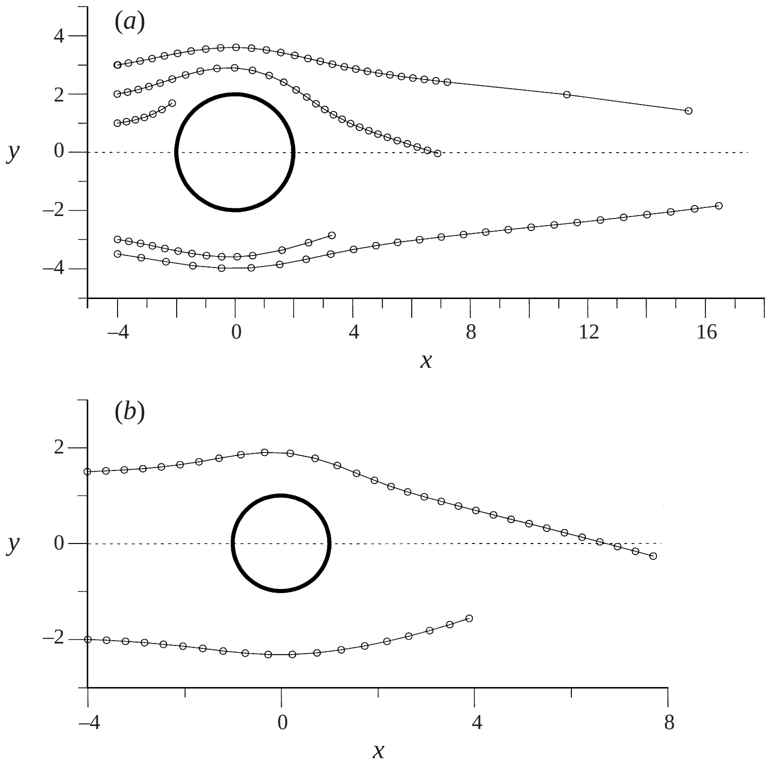

FIGURE 3. (*a*) Trajectories of piecewise-uniform vorticity eddies advected around an obstacle with $R = 2$, $U = 0.2$ and various $y_3(0)$. (x_3, y_3) are the coordinates of the cyclonic point vortex of the inner core. The plotted points on each trajectory do not necessarily correspond to equal time intervals. The last plotted point for $y_3(0) = 1$ corresponds to the strong interaction in figure 6(*b*), and the last point for $y_3(0) = -3$ corresponds to figure 5(*b*). (*b*) Same as in (*a*) except for a smaller obstacle ($R = 1$).

we maintained vorticity compensation at every time step by resetting $G = -\omega$ times the instantaneous area bounded by C_2. At $t = 16$ (in figure 2) there is a small dipole $x_3 - \overline{x} = 0.015$, but later on ($t = 50$), (when $x_3(50) = 5.187$), the separation increases to $x_3(50) - \overline{x}(50) = 0.050$. At this time the $y_3(t)$, $x_3(t)$ trajectory (figure 3) shows that the entire eddy has acquired a nearly constant transverse velocity:

$$\frac{\mathrm{d}y_3}{\mathrm{d}t} \approx \frac{y_3(56) - y_3(46)}{56 - 46} = \frac{-0.031 - 0.521}{10} = -0.0552. \tag{4.1}$$

In order to compare this with the theoretical value (equation (1.2)) for an isolated quasi-monopolar eddy, we use the average value of $x_3 - \overline{x}$ from $t = 46$ to $t = 56$ to obtain the mean dipole $D_x = (0.050 + 0.058)/2 = 0.054$, and substitution of this in (1.2) yields a value

$$V = \frac{0.054(-2)}{2} = -0.054, \tag{4.2}$$

in good agreement with (4.1). Thus we see how a ‘grazing’ incidence of the eddy around an obstacle results in a systematic increase in the dipole moment (or in the amplitude of the $m = 1$ azimuthal mode), thereby producing a finite scattering angle between the mean path of the eddy at $x \gg R$ and the mean field direction.

A smaller scattering angle is expected when $y_3(0) = \overline{y}(0)$ is increased to 3.0, as

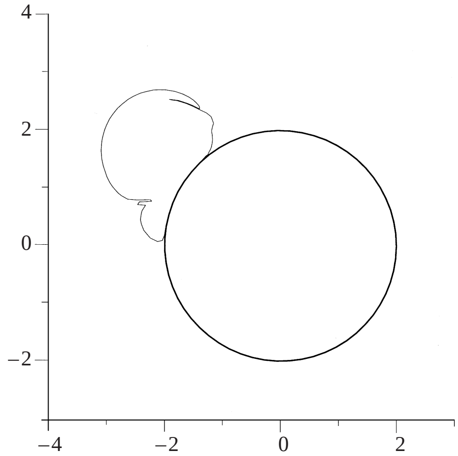

FIGURE 4. Same as figure 2 except $y_3(0) = \bar{y}(0) = 1$. At this time ($t = 12$) the eddy interface is in very close contact with the obstacle and the calculation is stopped (see text).

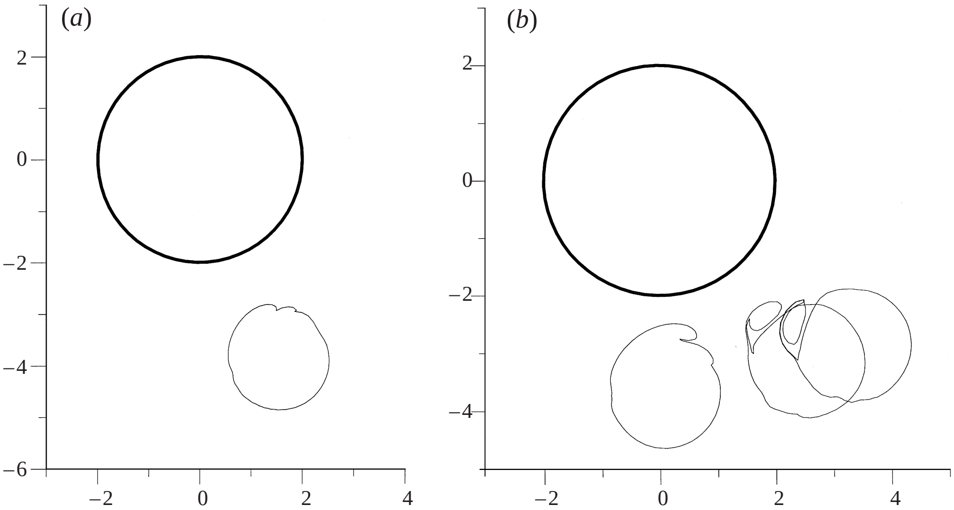

FIGURE 5. (*a*) A 'weak' interaction for $y_3(0) = -3.5$, $U = 0.2$, $R = 2$, $t = 24$. (*b*) A 'strong' interaction for $y_3(0) = -3$, $U = 0.2$, $R = 2$ is shown at three times. An essentially multi-connected domain forms as the eddy bifurcates into two parts connected by a thin filament which could clearly be removed ('surgerized').

is confirmed in figure 3. But when $y_3(0) = \bar{y}(0)$ is decreased to 1.0 (figure 4) the interaction is no longer weak, and the 'head on' collision which occurs at $t = 12$ is such that a significant fraction of C_2 comes into very close contact with the rigid boundary of the obstacle. Thus very large azimuthal velocities are subsequently induced (not shown) on C_2 due to the closeness of the ω images. Since our limited resolution of the subsequent evolution gave a tangled (and meaningless) mass of curves and filaments, the integration was stopped at $t = 12$; the subsequent evolution of the strong interaction (figure 4) is beyond our present scope.

The interaction for negative $y_3(0) = \bar{y}(0) = -3$ is much stronger than for positive $y_3(0) = +3$, as may be seen from the respective trajectories in figure 3. The $y_3(0) = -3$ interaction (figure 5*b*) is such that the eddy bifurcates into two essentially disconnected

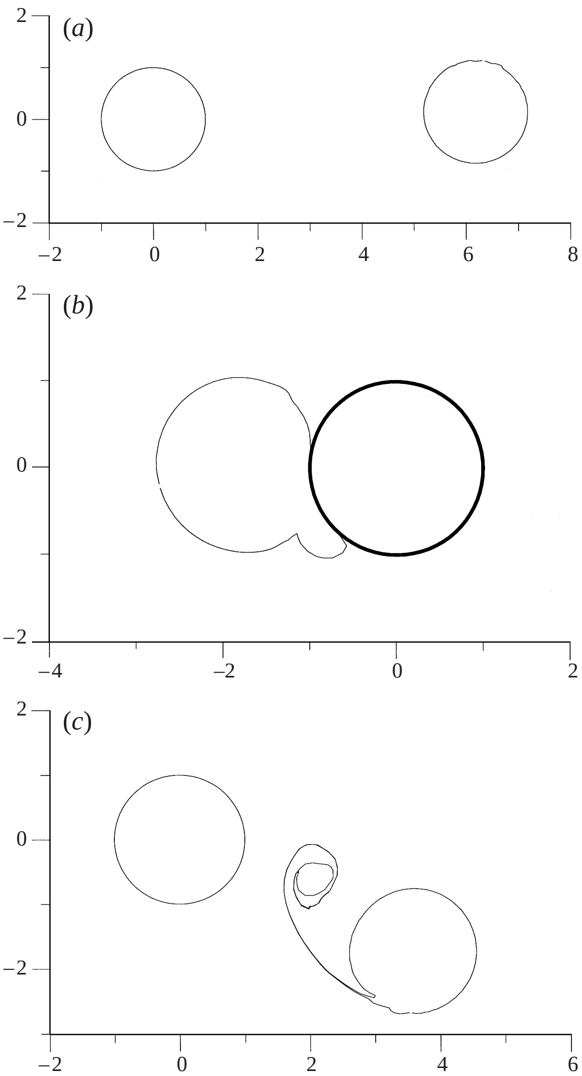

FIGURE 6. (*a*) $y_3(0) = 1.5$, $U = 0.2$, $R = 1$. At the time of this figure the eddy has been advected far downstream from the circular obstacle centred at $(0, 0)$. At the time when $x_3 \approx 0$ (not shown) the bottom of C_2 is 0.02 above the top of the $R = 1$ obstacle (grazing incidence), but the subsequent ($x_3 \gg 1$) evolution is still 'weak scattering'. (*b*) Same as (*a*) except $y_3(0) = 0$. A 'head on' collision occurs with C_2 coming into very close contact with $R = 1$. (*c*) Same as previously except $y_3(0) = -2.0$. The cyclonic rotating eddy bifurcates in the lee of the obstacle.

domains, a topological change which falls into our definition of 'strong interaction'. On the other hand 'weak' scattering occurs (figure 5*a*) when $y_3(0) = \overline{y}(0)$ is decreased to -3.5. The far-field value of $\mathrm{d}y_3/\mathrm{d}t$, computed from figure 3 also agreed with the theoretical prediction (equation (4.2)) to 2%. Figure 3 implies that there is a critical value of $y_c = |y_3(0)| = |\overline{y}(0)|$ above which weak scattering occurs; for $R = 2$, $U = 0.2$ the approximate value is $y_c \approx 1.5$ (for positive $y_3(0)$), and $y_c \approx 3.25$ (for negative $y_c(0)$).

For a smaller $R = 1$, figures 3(*b*), 6(*c*) imply that y_c is somewhat less than 1.5 for $y_3(0) > 0$, and somewhat less than -2.0 for $y_3(0) < 0$. Aside from the quantitative

R	U	$y_3(0)$	final $x_3 - \overline{x}$	Comment
1	0.15	1.5	+0.060	@ $t = 88$, one eddy
				* * * * *
1	0.075	1.5		'catastrophic' collision; close contact with obstacle @ $t = 48$, $x_3 = -0.28$
1	0.20	1.5	+0.052	@ $t = 60$
2	0.20	2	+0.058	@ $t = 56$
2	0.20	3	+0.030	@ $t = 92$
2	0.20	1		catastrophic collision @ $t = 16$
2	0.20	−3.5	−0.27	@ $t = 104$, one eddy
				* * * * *
2	0.20	−3.0		bifurcation into two eddies
1	0.20	−2.0		bifurcation into two eddies
0.5	0.20	−1.5		bifurcation into two eddies
1	0.20	0		catastrophic collision

TABLE 1. Parametric variation of scattering. The line of asterisks indicates the point of transition from weak to strong scattering.

difference between $R = 2$ and $R = 1$, figure 6 shows the similar topological regimes in the two cases, namely weak scattering (figure 6*a*), head on collision (figure 6*b*), and bifurcation (figure 6*c*). The summary table 1 shows that a strong interaction occurs even for $R = 0.5$.

5. The centroid invariance theorem for baroclinic eddies

For reasons mentioned in the introduction, we conclude by deriving a new centroid invariance theorem for quasi-geostrophic baroclinic eddies. Consider a two-layer density model bounded by rigid and flat upper and lower boundaries, and with an intervening density interface. Let H_1 denote the mean thickness of the upper layer (density ρ), H_2 the mean thickness of the lower layer (density $\rho + \Delta\rho$), and $h(x, y, t)$ the upward displacement of the interface from its undisturbed position. In the limit when $|h|/H_1 \ll 1$, and when the Rossby number is equally small, we obtain the well known quasi-geostrophic (QG) approximation (Stern 1975). If f is the (constant) Coriolis parameter, and $[\omega_1(x, y, t), \omega_2]$ denotes the respective values of relative vorticity $(\partial v/\partial x - \partial u/\partial y)$ in each layer, then the QG 'potential vorticities' defined by

$$P_1 = \frac{\omega_1(x, y, t)}{f} + \frac{h}{H_1}, \quad P_2 = \frac{\omega_2}{f} - \frac{h}{H_2} \tag{5.1a, b}$$

are conserved with respect to non-divergent horizontal velocity (u, v) in each layer, i.e. $\partial u/\partial x + \partial v/\partial y = 0$. For a shielded eddy (far-field (x, y) velocities smaller than order $(x^2 + y^2)^{-1/2}$) we then obtain

$$\iint_{-\infty}^{+\infty} v_1\omega_1 \mathrm{d}x\,\mathrm{d}y \equiv \iint_{-\infty}^{+\infty} v_1 \left(\frac{\partial v_1}{\partial x} - \frac{\partial u_1}{\mathrm{d}y}\right) \mathrm{d}x\,\mathrm{d}y = 0, \tag{5.2a}$$

and

$$\iint_{-\infty}^{+\infty} v_2\omega_2 \mathrm{d}x\,\mathrm{d}y = 0. \tag{5.2b}$$

When (5.1a) is multiplied by $H_1 v_1$, and (5.1b) is multiplied by $H_2 v_2$, and when (5.2a, b) are used we get

$$I \equiv \iint \mathrm{d}x\,\mathrm{d}y(H_1 v_1 P_1 + H_2 v_2 P_2) = \iint \mathrm{d}x\,\mathrm{d}y(v_1 h - v_2 h). \tag{5.3}$$

Since the motion is geostrophic and hydrostatic, the 'thermal wind' (Margules Relation) equation is

$$v_1 - v_2 = \frac{(g\Delta\rho/\rho)}{f}\frac{\partial h}{\partial x},$$

where g is gravity. Equation (5.3) therefore reduces to $I = 0$, or, equivalently

$$I = \iint \mathrm{d}\sigma H_1 P_1 \left(\frac{\mathrm{d}y_1}{\mathrm{d}t}\right) + \iint \mathrm{d}\sigma H_2 P_2 \left(\frac{\mathrm{d}y_2}{\mathrm{d}t}\right) = 0,$$

where v_1 and v_2 have been written as Lagrangian derivatives and $\mathrm{d}\sigma = \mathrm{d}x\,\mathrm{d}y$.

A material column in each layer not only conserves P, but also, according to the QG approximation, conserves its cross-sectional area ($\mathrm{d}\sigma$). Therefore we may take the time derivative in the above equation outside the integral to obtain

$$\frac{\partial}{\partial t}\left[\iint_{-\infty}^{+\infty} \mathrm{d}\sigma H_1 P_1 y_1 + \iint_{-\infty}^{+\infty} \mathrm{d}\sigma H_2 P_2 y_2\right] = 0,$$

or

$$0 = \frac{\partial}{\partial t}\iint_{-\infty}^{+\infty} \mathrm{d}x\,\mathrm{d}y(H_1 P_1 + H_2 P_2)y = \frac{\partial}{\partial t}\iint \mathrm{d}x\,\mathrm{d}y(H_1\omega_1 + H_2\omega_2)y, \tag{5.4}$$

where (5.1a, b) have been used. Therefore the centroid of the barotropic component of the relative vorticity, i.e. the vertically integrated part of the total baroclinic flow is invariant if there are no external boundary forces. Thus we see that even when a deep bottom layer has a relatively small $|\omega_2|$, this layer can exert a control on the entire baroclinic evolution because $H_2 \gg H_1$. The question then arises as to whether a finite integral value of $(H_1\omega_1 + H_2\omega_2)y$ in an otherwise circularly symmetric eddy can be generated if it is advected towards a sea mount in the bottom layer.

6. Conclusion

We have considered a compact (shielded) two-dimensional eddy consisting of negative (say) vorticity in an outer annulus, and compensating positive vorticity in an inner domain. The separation of the centroids of the two vorticity domains is known to be independent of time unless external forces, such as is due to topographic pressure, are present. We have shown that if a circularly symmetric eddy, initially at $x = -\infty$, is advected by uniform current (U) towards an obstacle of radius R (centred at $x = 0$), then the centroid of the negative (say) vortices in the outer part of the eddy is displaced from the centroid of the positive interior vortices. For 'grazing' incidence (weak scattering) the eddy is advected around the obstacle and emerges far downstream with a small dipole moment which allows the eddy to maintain a velocity normal to the free stream.

A 'head-on collision' occurs when the magnitude of the initial y-distance between the centre of the eddy and the (nearest) topographic extremum ($y = \pm R$) is less than a critical value, an estimate of which has been given. Such a strong interaction results in a topological change of the eddy, as implied by figures 4, 6 or by figures 5(b), 6(b).

The extension to the more realistic oceanic case of a rotating fluid with multiple density layers is suggested by the generalization (§ 5) which shows that the centroid of the barotropic (vertically integrated) vorticity is invariant when external forces are absent. When a sea mount and a basic current are added to this problem, we expect that finite value of the 'invariant' will be generated by the pressure exerted by the eddy on the obstacle. Of course if the eddy has a finite initial dipole moment, then this may be increased by the encounter.

Partial support by NSF grants OCE9529261 and OCE9726584 is gratefully acknowledged.

REFERENCES

Beismann, J. D., Käse, R. H. & Lutejeharms, J. R. E. 1999 On the influence of submarine ridges on translation and stability of Agulhas rings. *J. Geophys. Res.* **104**, 7897–7906.

Carnevale, G. F., Kloosterziel, R. C. & Heijst, G. J. F. van 1991 Propagation of barotropic vortices over topography in a rotating tank. *J. Fluid Mech.* **233**, 119–139.

Flierl, G. R. 1988 On the instability of geostrophic vortices. *J. Fluid Mech.* **197**, 349–388.

Richardson, P. L. & Tychensky, A. 1998 Meddy trajectories in the Canary Basin. *J. Geophys. Res.* **103**, 25 029–25 045.

Rott, N. 1989 Three vortex motion with zero circulation. *Z. Angew. Math. Phys.* **40**, 473–494.

Saffman, P. G. 1992 *Vortex Dynamics*. Cambridge University Press. 311 pp.

Stern, M. E. 1975 *Ocean Circulation Physics*. Academic. 246 pp.

Stern, M. E. & Radko, T. 1998 The self-propagating quasi-monopolar vortex. *J. Phys. Oceanogr.* **28**, 22–39.